Journal of Physics and Chemistry of Solids 136 (2020) 109137

Contents lists available at ScienceDirect

Journal of Physics and Chemistry of Solids

journal homepage: www.elsevier.com/locate/jpcs

Electronic structure and magnetism of the 35 K superconductor $CsEuFe_4As_4$

Farshad Nejadsattari[a], Mohammed A. Albedah[a,b], Zbigniew M. Stadnik[a,*]

[a] Department of Physics, University of Ottawa, Ottawa, Ontario, K1N 6N5, Canada
[b] Department of Physics, Majmaah University, P.O. Box 1712, Zulfi, Saudi Arabia

ARTICLE INFO

Keywords:
Density of states
Energy band structure
Magnetic moment
Hyperfine interaction

ABSTRACT

The results of *ab-initio* calculations of the electronic structure and magnetism of the new 35 K superconductor $CsEuFe_4As_4$ are reported. The electronic band structure and the density of states are presented and discussed in detail. The origin of the chemical bonding between the constituent atoms is discussed in detail. The evidence is provided for the existence of a mixture of ionic, covalent, and metallic bonding. It is demonstrated that the magnetic moment is mainly due to the strongly localized Eu *f* states. No spin polarization at the Fe sites is found. It is demonstrated that the electrical conductivity in $CsEuFe_4As_4$ originates from the Fe contribution to the density of states. The electrical and chemical properties of the studied compound are closely linked with the presence of the Fe *d* states in the Fermi energy region. The Fermi surfaces show the presence of the hole-like and electron-like pockets, respectively, at the center and corners of the Brillouin zone. The results of the calculations of the ^{57}Fe and ^{151}Eu hyperfine-interaction parameters are also presented.

1. Introduction

The discovery of a new Fe-based class of superconductors $AeAFe_4As_4$ (*Ae*= Ca, Sr, Eu and *A*= K, Rb, Cs) with the critical temperature T_c in the range 31.6–36.8 K [1–4] is significant for two reasons. First, in contrast to the intensively studied solid solutions of $(Ba_{1-x}K_x)Fe_2As_2$ or $(Sr_{1-x}Na_x)Fe_2As_2$, the *Ae* and *A* atoms in $AeAFe_4As_4$ are located at the crystallographically inequivalent positions, which causes the change of the space group from $I4/mmm$ characteristic for solid-solution superconductors to $P4/mmm$. In these new superconductors, the *Ae* and *A* layers are alternately stacked along the crystallographic *c*-axis between the Fe_2As_2 slabs. Consequently, the absence of structural disorder in $AeAFe_4As_4$ allows for the investigations of their intrinsic physical properties that are not hindered by the structural disorder present in solid-solution superconductors. Second, the presence of the Eu and Fe atoms, which potentially can order magnetically, points toward the possibility of the coexistence of two, generally incompatible phenomena, magnetism and superconductivity [5].

The magnetic susceptibility measurements [2,4] indicate that the $CsEuFe_4As_4$ superconductor with T_c= 35.1–35.2 K has a magnetic transition at ~15.0–15.5 K. Such a magnetic transition has also been found in the heat capacity data at 15.2 K [4] and at 15.97 (8) K in the ^{151}Eu Mössbauer data [6]. The isothermal magnetization data made it possible to identify this transition as being ferromagnetic [4]. Ferromagnetism in $CsEuFe_4As_4$ has been hypothesized [4] to be associated only with the Eu magnetic moments, that is, it has been assumed that the Fe atoms have no magnetic moment. These suggestions have been confirmed experimentally in the ^{151}Eu and ^{57}Fe Mössbauer study of $CsEuFe_4As_4$ [6].

The main goal of this work is to elucidate the origin of some of the physical properties of $CsEuFe_4As_4$ via detailed electronic structure calculations. In particular, the formation and type of chemical bonds in this compound and the charge transport properties are studied. The type of chemical interactions between various atoms in $CsEuFe_4As_4$ are similar to those observed in other compounds of the same crystallographic structure [7]. A thorough discussion of the Fermi surface topology allows for the understanding of the electronic characteristics of $CsEuFe_4As_4$. Furthermore, a framework to test and, to some extent, predict the properties of this compound is provided. A comparison is made between the calculated physical quantities and those obtained from the magnetic and Mössbauer spectroscopy measurements.

2. Theoretical method

We performed *ab initio* calculations of the electronic structure and Mössbauer hyperfine-interaction parameters of $CsEuFe_4As_4$ in the context of density functional theory using the full-potential linearized augmented-plane-wave plus local orbitals (FP-LAPW + lo) method that is realized in the WIEN2k package [8]. This method is described thoroughly in Ref. [9]. Here, the valence wave functions in the interstitial

* Corresponding author.
E-mail address: stadnik@uottawa.ca (Z.M. Stadnik).

https://doi.org/10.1016/j.jpcs.2019.109137
Received 21 May 2019; Received in revised form 20 July 2019; Accepted 5 August 2019
Available online 07 August 2019
0022-3697/

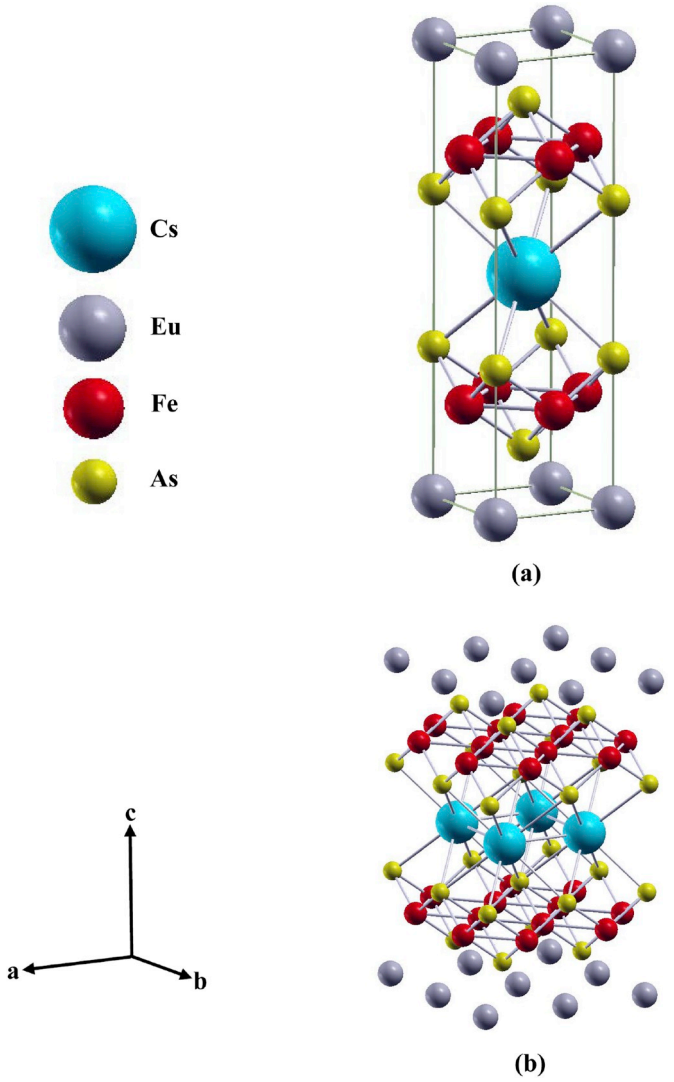

Fig. 1. (Color online) The unit cell (a) and the layered crystal structure (b) of $CsEuFe_4As_4$. (For interpretation of the references to colour in this figure legend, the reader is referred to the Web version of this article.)

region are expanded in spherical harmonics up to $l = 4$, while in the muffin-tin (MT) region they are expanded to a maximum of $l = 10$ harmonics. The values of 2.50, 2.50, 2.30, and 2.19 a.u. were used as the muffin-tin radii for Cs, Eu, Fe, and As, respectively. For the exchange-correlation potential, the generalized gradient approximation (GGA) scheme of Perdew, Burke, and Ernzerhof [10] was used. In addition, effective Hubbard-like interaction energies of 0.52 and 0.15 Ry were used for the Eu 4*f* and Fe 3*d* states, respectively [7,11]. The plane-wave cut-off parameter was set to $R_{MT} \times K_{MAX} = 7.0$, where R_{MT} is the smallest MT radius in the unit cell and K_{MAX} is the maximum K vector used in the plane-wave expansion in the interstitial region. A total number of 680 inequivalent k-points was used within a $32 \times 32 \times 9$ k-mesh in the irreducible wedge of the first Brillouin zone. The experimental lattice parameters (a and c) and the atomic position parameters from Ref. [6] were employed in the calculations.

3. Results and discussion

3.1. The crystal structure

Fig. 1 shows the unit cell and the layered crystal structure of $CsEuFe_4As_4$. Various connecting rods represent the interactions between the Cs, Fe, and As atoms. One can notice that the layers of Eu atoms are entirely isolated from the Fe_4As_4 blocks and that the sheets of Cs atoms along the c-direction separate the neighboring Fe_4As_4 blocks [6].

The layered structure and the network of the connecting rods [Fig. 1 (b)] point towards the existence of a combination of covalent and ionic bonds (*vide infra*) in the compound studied [6].

3.2. Ab-initio Calculations

3.2.1. Valence charge density distributions

The valence charge density distributions along various planes are shown in Fig. 2. The electronic charges of the atoms in $CsEuFe_4As_4$ were obtained through the Bader's analysis scheme [12]. The presence of a combination of ionic, covalent, and metallic bonds between various atoms in $CsEuFe_4As_4$ becomes evident by inspecting Fig. 2 in detail.

As one can notice from the charge density distribution in the (001) plane [Fig. 2(a)], there is the absence of valence charge in the regions between the Eu atoms (red regions). This indicates that the Eu atoms are chemically isolated from each other. Therefore, no chemical bonding is expected to exist between these atoms. This is depicted in Fig. 1 by the lack of connecting rods between the Eu atoms, which supports the argument given above. One also observes [Fig. 2(a)] that the valence electrons of Eu are strongly bound to the parent atom (the yellow, green, and blue rings surrounding each Eu atom). Furthermore, a fourth-fold shape of the half-filled 4*f* shell of Eu is evident [purple regions in Fig. 2(a)].

The valence charge density distribution in the (002) plane is shown in Fig. 2(b). This plane consists of sheets of Cs atoms which separate the neighboring Fe_4As_4 blocks in the c-direction. One can see that the charge density distribution around the Cs atoms is perfectly symmetric. In fact, what is shown in this figure is the closed shell structure of the Xe atom, with the *s* electrons of Cs completely transferred from their parent atom to the Fe_4As_4 blocks, in particular, to the As atoms. These electrons participate in the ionic bonding between the Cs sheets and the Fe_4As_4 blocks. The Cs atoms themselves are isolated from each other due to their relatively large separation. Consequently, no metallic interaction is likely to exist between them.

Fig. 2(c) shows the valence charge density distribution in the $z = 0.6726$ plane which consists of the As atoms located at the 2*g* sites. The presence of a very weak directional covalent bonding between the adjacent As atoms can be seen (faint yellow regions). These As atoms are isolated from each other by regions which have virtually no charge density. However, the As atoms located at the 2*h* sites [Fig. 2(d)] are involved in forming stronger covalent bonding with the neighboring Fe atoms [the $z = 0.6726$ plane in Fig. 2(d) passes through the Fe layers]. The valence charge density distribution in this plane indicates that the electronic charge is spread out between the Fe–Fe and Fe–As atoms. The Fe–Fe interactions are realized by forming metallic bonds as the Fe 4*s* electrons are widely spread throughout the Fe layers [green regions in Fig. 2(d)]. The electronic transport in the superconductor studied is expected to occur predominantly within these Fe layers and, to a smaller extent, within the metallic Fe_4As_4 blocks.

The valence charge density distribution in the (110) plane is shown in Fig. 2(e). This plane passes through the Eu and Cs atoms, and also through the As atoms located at the 2*h* sites. The presence of the As–As covalent bonds is clearly visible as the electrons are delocalized between these atoms (green regions). Furthermore, a complete charge transfer from the Cs and Eu atoms to the As layers is evident (red regions indicating the virtual absence of charge). This leads to the formation of two sets of ionic bonds: a strong ionic bond between the alkali Cs layers and the metalloid As layers, and a weaker ionic bond between the layers of the Eu and As atoms. One can interpret this result by considering the differences between the electronegativity of the Cs (0.79) and the Eu (1.2) atoms and that of the As (2.18) atoms. Based on these electronegativity values, the Cs–As bond is expected to be

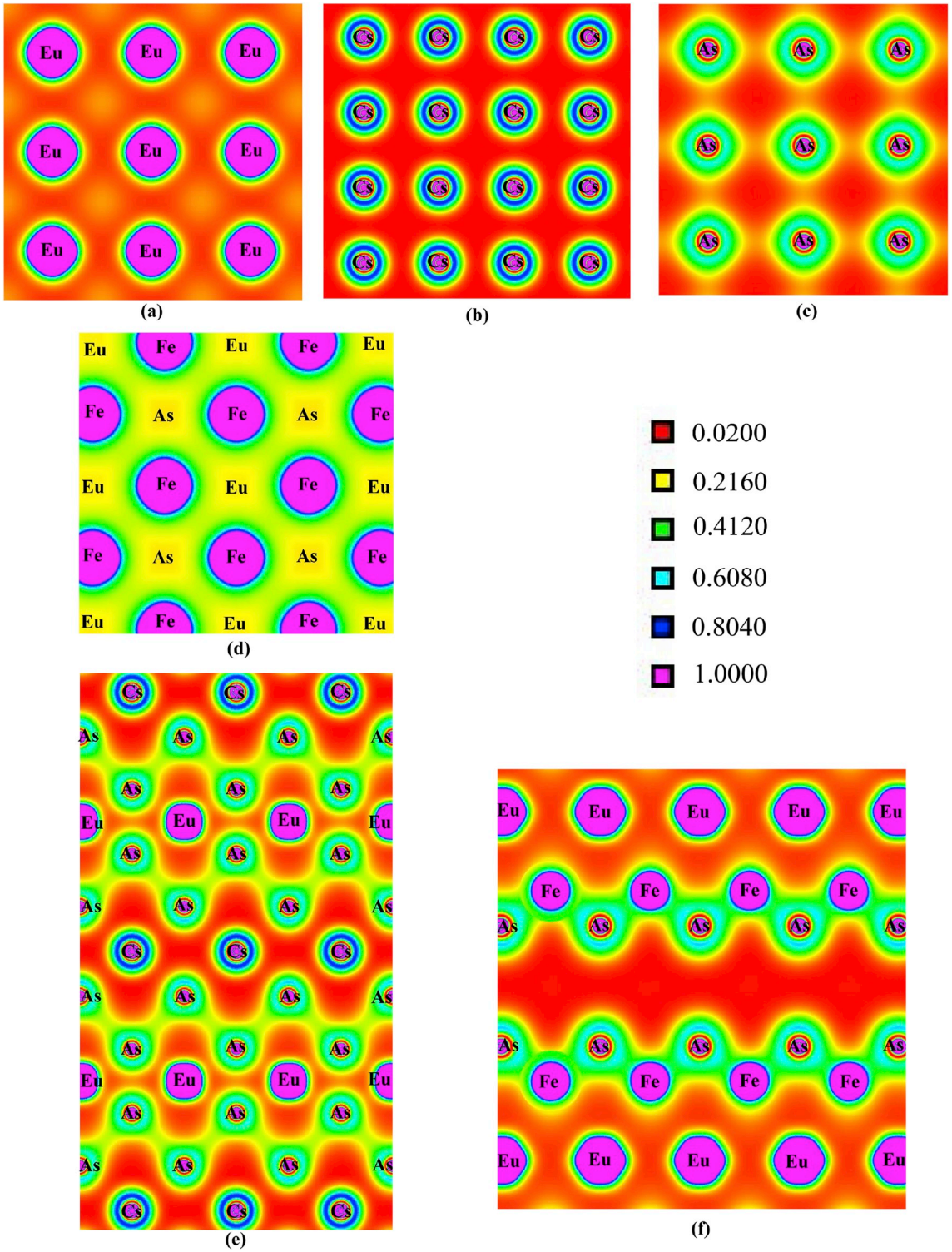

Fig. 2. (Color online) Electron charge density distribution (in units of e/Å^3) along the (001) (a), (002) (b), $z = 0.6726$ (c), $z = 0.7738$ (d), (110) (e), and (010) [(100)] (f) planes. (For interpretation of the references to colour in this figure legend, the reader is referred to the Web version of this article.)

stronger than the Eu–As bond. These two sets of ionic bonding are depicted in Fig. 2(e) by two red regions of different intensity. No electronic transport is expected to exist between the separate As layers due to the formation of these ionic bonds. As mentioned earlier, any transport (whether electrical or thermal) must be along the Fe_4As_4 blocks.

If one considers the symmetry of the space group $P4/nmm$ and the crystal basis of $CsEuFe_4As_4$, then it becomes clear that the charge density distributions in the (010) and (100) planes are the same [Fig. 2(f)]. These planes pass through the Eu, As at the 2*g* sites, and Fe atoms. A careful inspection of this figure reveals the hexagonal shape of the cross-section of the Eu 4*f* orbitals with these planes. One also notices that the sheets of Eu atoms are separated from each other (the virtual absence of charge density indicated by red regions). The strong covalent As–Fe bonds are visible in the figure via delocalization of the valence states of the As and Fe atoms. This is indicated [Fig. 2(f)] by the

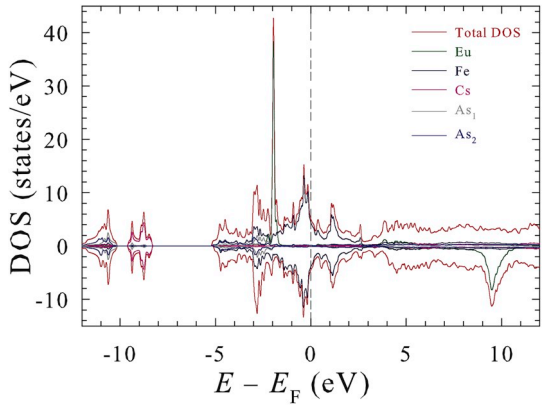

Fig. 3. (Color online) Spin-resolved, total and atom-resolved DOS in ferromagnetic $CsEuFe_4As_4$. (For interpretation of the references to colour in this figure legend, the reader is referred to the Web version of this article.)

presence of a comparatively high charge density (green regions which spread in between the As and Fe atoms).

3.2.2. Density of states

In this section, we bring the results of the DFT calculations for the total and partial density of states (DOS) in $CsEuFe_4As_4$. The integration in the *k*-space was done using the modified tetrahedron method [13].

The DOS below −8 eV (Fig. 3) is due to the atomic-like core electrons of Cs and As atoms. As these core states lie deep in energy, they practically do not contribute to any of the physical properties of the compound studied. In fact, the DOS of these states resembles that of isolated atomic states of the Cs and As atoms.

The DOS in the energy region between −5.0 and 2.8 eV, which includes the Fermi energy (E_F), determines most of the physical properties of $CsEuFe_4As_4$. Here the semi-core, valence, and conduction states form a continuum of DOS. A local minimum in the DOS at ~0.7 eV indicates the presence of a pseudogap that is due to a few Fe states. This pseudogap can be attributed to the Coulomb repulsion of the Fe electrons. The energy region between − 1.5 eV and E_F is dominated by the delocalized Fe states. They form a valence band that is responsible for the formation of the metallic bonds between the Fe atoms within the Fe_4As_4 blocks. A sharp peak in the spin-up DOS in the energy region between − 2.0 and − 1.6 eV arises entirely from the localized Eu *f* electrons. The Eu *f* states have minimum overlap with the Fe *d* states. Below the energy region dominated by the Eu *f* states (between − 3.1 and − 2.1 eV), one observes contributions from the As and Fe atoms. The overlap between the As and Fe states in this region is indicative of covalent bonding between the As and Fe atoms. This covalent bonding is the result of the hybridization between the Fe *d* states with those of the As *p* states.

A characteristic feature of the DOS in Fig. 3 is that, in contrast to the energy separation and magnitude difference between the Eu spin-up and spin-down states, the spin-up and spin-down DOS contributions from the other atoms is symmetric. This results in almost negligible magnetic moments of the Cs, Fe, and As atoms (*vide infra*). As a consequence of the high asymmetry observed in the Eu DOS from its two spin components, a large magnetic moment of the Eu atoms is expected.

The near Fermi energy region is dominated by the Fe *d* states and, to a far less extent, by the As *p* states. These states are ultimately responsible for the conductive nature of $CsEuFe_4As_4$. There is almost zero DOS contribution from the Eu and Cs atoms in the Fermi energy region. This suggests that the conductivity in $CsEuFe_4As_4$ must be confined to the Fe–As layers, and thus is anisotropic.

Fig. 4(a) displays the spin-resolved DOS due to the Cs atoms. The symmetry of the spin-up and spin-down states is evident. Consequently, one expects no magnetic moment for the Cs atoms in $CsEuFe_4As_4$. One also observes that there is virtually no Cs contribution to DOS in the

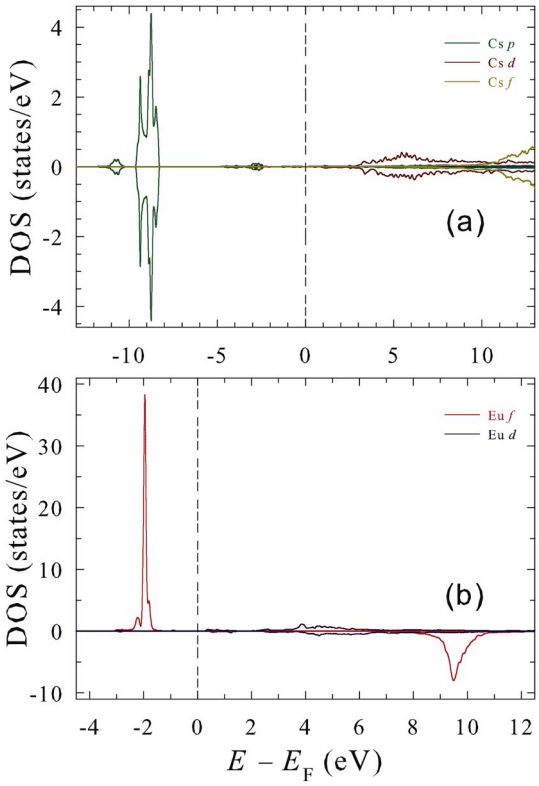

Fig. 4. (Color online) Spin-resolved DOS of the Cs (a) and Eu (b) atoms in ferromagnetic $CsEuFe_4As_4$. (For interpretation of the references to colour in this figure legend, the reader is referred to the Web version of this article.)

Fermi energy region. The core states of Cs are of the *p* character, and their DOS has three peaks at − 9.4, − 8.7, and − 8.5 eV in the energy region between − 9.8 and − 8.3 eV. The much smaller DOS due to the core Cs *p* states is also in the other energy region between − 11.5 and − 8.5 eV.

A highly localized DOS due to the Eu *f* states, as opposed to the extended one due to the Eu *d* states, can be seen in Fig. 4(b). The contribution to DOS from the Eu *d* states is minimal and symmetric for both spin orientations, whereas that from the Eu *f* is very large and asymmetric. The majority spin contribution is from the sharp *f* up states of Eu that are localized between − 2.4 and − 1.5 eV. On the other hand, the minority *f* down states of Eu lie in a relatively high-energy region (between 8.6 and 10.5 eV). Under normal conditions, these states are empty as no electron can have enough energy to occupy them. This significant difference in the population of the two spin configurations accounts for a large magnetic moment found experimentally in $CsEuFe_4As_4$ [4]. The majority of the Eu *d* states also lie above E_F. Though few, they are widely spread between 3.2 and 8.5 eV.

One observes an overlap between the Fe *s* and *p* states 3.2 eV [Fig. 5(a)]. Below E_F, these states are fairly separated with several peaks in the DOS. A small contribution of the Fe core states to the DOS is in the energy region between − 12 and − 10 eV. One notices that the Fermi energy region is almost empty of the Fe *s* and *p* states.

As mentioned earlier, the most significant contribution to the Fe DOS originates from the *d* orbitals. Fig. 5(b) displays the individual *d*-orbital-resolved contributions to the Fe *d* DOS. It is evident that the large peak in the Fe DOS originates mainly from the $d_{x^2-y^2}$ states located at about eV. These states are mainly localized and exist below E_F. The small peak in the DOS above E_F at about 1.0 eV originates from the d_{xy} and d_{z^2} orbitals. The d_{z^2} states also extend to the region below E_F and they peak at around − 0.5 eV. The majority of the d_{xz} states are located in the vicinity of E_F and contribute to the peak at − 0.15 eV. The conductive nature of $CsEuFe_4As_4$ can be related to these states. The

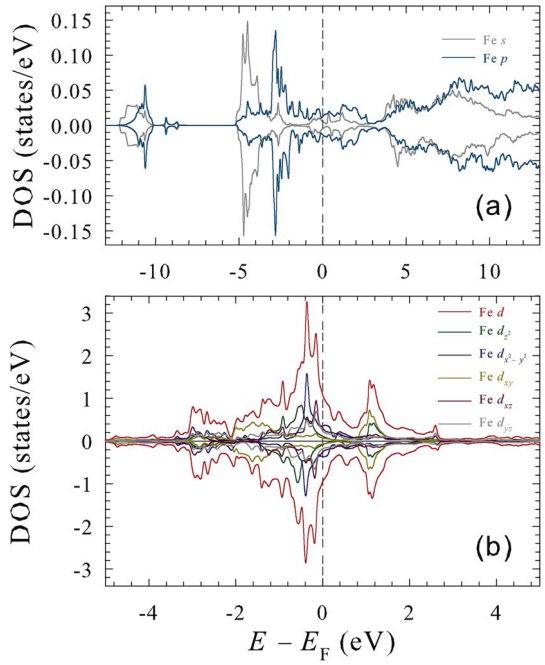

Fig. 5. (Color online) Spin-polarized, Fe orbital-resolved DOS (a) and Fe *d*-orbital-resolved DOS (b). (For interpretation of the references to colour in this figure legend, the reader is referred to the Web version of this article.)

smallest contribution to the Fe *d* DOS is from the d_{yz} states which are non-localized and predominantly spread below E_F into the valence region.

Fig. 6(a) displays the DOS due to the As_1 and As_2 atoms located at two different Wyckoff positions 2*g* and 2*f*, respectively [6]. One can notice that although the states due to the As_1 and As_2 atoms occupy the same energy region, they are slightly displaced from each other. The As

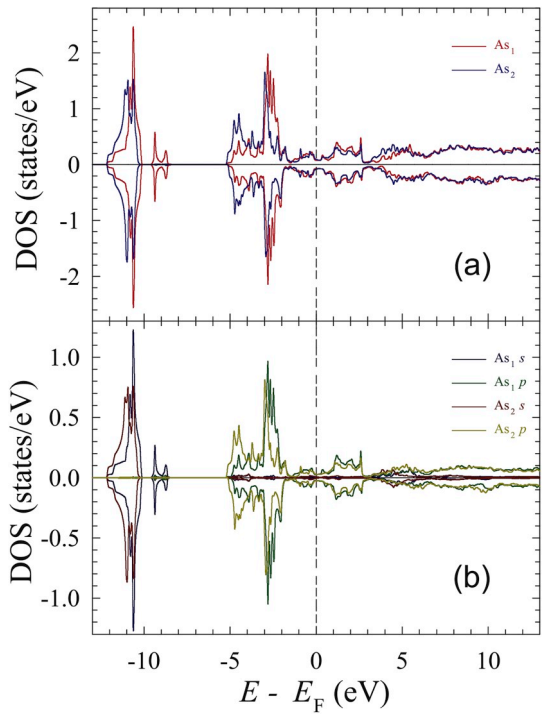

Fig. 6. (Color online) Spin-resolved DOS of As (a) and spin-resolved, orbital-resolved DOS of As. (For interpretation of the references to colour in this figure legend, the reader is referred to the Web version of this article.)

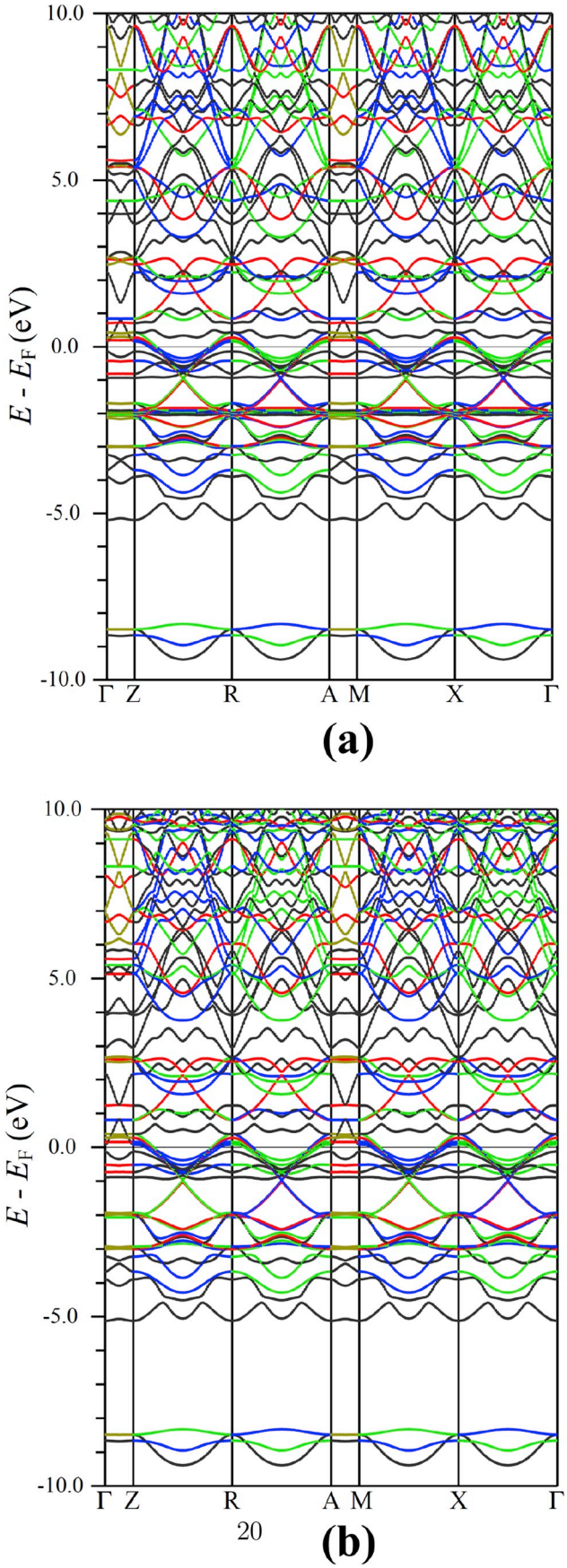

Fig. 7. (Color online) Spin-up (a) and spin-down band structures of ferromagnetic $CsEuFe_4As_4$. (For interpretation of the references to colour in this figure legend, the reader is referred to the Web version of this article.)

core states lying between − 12 and − 10 eV are localized and are of atomic-like character. The semi-core and valence states span an energy region between − 5.0 and − 1.6 eV and display sharp peaks in DOS between − 3.0 and − 2.7 eV. The conduction states extend from E_F to 2.8 eV. Above 2.8 eV, the mainly empty metallic, and perfectly overlapping As_1 and As_2 states are located. As a result of the presence of non-localized and overlapping states, the bonding between the As atoms in the compound studied is covalent.

As one can observe in Fig. 6(b), the core states lying deep in energy consist of *s*-type orbitals whereas the states close to E_F are dominated by the relatively extended *p* states (between − 5.2 and − 1.7 eV). The As_1 states are slightly more numerous than the As_2 states. The spin-up and spin-down contributions to the DOS from both atoms are almost identical, which yields nearly zero magnetic moments of the two As atoms.

3.2.3. Energy band structure

One can observe that for the spin-up configuration [Fig. 7(a)], the energy bands above E_F are greatly dispersive. In the vicinity of E_F, the bands are less dispersive. The bands at − 2 eV are very dense and flattened. They originate from the Eu *f* states. The small dispersion of these bands indicates that they correspond to the extremely localized states. The small curvature of the bands points to a large corresponding effective mass m^* ($m^* \sim [\nabla^2_{\mathbf{k}} E(\mathbf{k})]^{-1}$), that is, the carriers occupying these bands are essentially immobile.

The characteristics of the bands for the spin-down configuration [Fig. 7(b)] are essentially the same as those for the spin-up configuration. The only difference is in the Eu *f* states that lie now high above E_F (at ~10 eV) and are numerous and flat. Similarly to the spin-up configuration, the E_F region is dominated by the Fe *d* states.

A common feature that can be observed for both spin-up and spin-down configurations (Fig. 7) is the merging of the energy bands along the high-symmetry points in the Brillouin zone, such as Γ, X, and R. As one moves away from these points, the symmetry on the *k*-space is broken and consequently the bands start to diverge from each other. The electronic states along these high-symmetry directions are localized and nested because any carrier in these regions will be subject to a null net electrostatic force, thus confining the carriers into regions in the vicinity of these special points.

3.2.4. Atom-resolved energy band structure

The spin-polarized, energy bands originating from the Fe, Eu, Cs, As_1, and As_2 atoms are presented in Fig. 8. In this figure, the thickness of the bands indicates their relative weight, that is, their relative contribution to the energy band structure of $CsEuFe_4As_4$. One can notice that the majority of the Fe energy bands [thick lines in Fig. 8(a) and (b)] lie in the vicinity and slightly below E_F. As mentioned earlier, they are mainly of the *d* character. The contributions from these states become smaller (represented by thinner lines), as one moves away from the E_F region in both directions.

There is a large difference between the spin-up and spin-down Eu energy bands [Fig. 8(c) and (d)], both in energy and in weight (thickness of the bands). This will lead eventually to a large magnetic moment carried by the Eu atoms. The energy bands for a spin-up configuration [Fig. 8(c)] are mainly confined to the energy region around − 2 eV, whereas for a spin-down configuration [Fig. 8(d)] the numerous Eu *f* bands are located above 9 eV. This observation is consistent with an earlier discussion of the DOS originating from the Eu *f* states. In both figures in the energy region above 5 eV, a smaller but symmetric contribution from the Eu 3*d* states is observed.

As one can notice in Fig. 8(e) and (f), the largest contribution to the band structure due to the Cs states is in the atomic energy region as indicated by the thick bands between − 9.5 and − 8.5 eV. The contributions from both spin configurations are identical along all directions in the Brillouin zone, and consequently, the magnetic moment of the Cs atoms in $CsEuFe_4As_4$ is negligible. A careful examination of Fig. 8(e) and (f) shows that there is a small contribution from the Cs energy bands across E_F (as indicated by the thin energy bands).

At first glance at Fig. 8(g)−(j) one can notice that the As_1 and As_2 atoms do not contribute significantly to the energy band structure of the compound studied. There are, however, two energy regions in which the As contribution is not negligible. The first energy region is in the neighborhood of E_F. Here, although the bands are thin, they are thicker than the rest of the bands. The other energy region is around − 2 eV.

3.2.5. Orbital-resolved energy band structure of Fe

Fig. 9 shows the spin-polarized band structure resulting from various Fe *d*-orbitals. One observes that the $d_{x^2-y^2}$ orbitals [Fig. 9(a) and (b)] dominate the E_F region. Multiple hole-like bands exist around the high symmetry points Γ, X, M, A, and R. Four regions of electron-like bands are observed midway between the connecting high symmetry directions Γ−X, M−X, A − R, and R − Z. One also observes a negligible dispersion along the A − M and Γ − Z directions.

The bands originating from the d_{z^2} orbitals [Fig. 9(c) and (d)] are similar to those due to the $d_{x^2-y^2}$ orbitals. However, they exhibit less dispersion across the Fermi level. Moreover, a fraction of these bands occupies another energy region below E_F (between − 0.9 and − 0.5 eV).

Most of the bands origination from the d_{xy}-orbitals are in the conduction region between 0.9 and 1.0 eV [Fig. 9(e) and (f)]. The contribution to the band structure of $CsEuFe_4As_4$ from the d_{xy} orbitals [Fig. 9(g) and (h)] and the d_{yz} orbitals [Fig. 9(i) and (j)] is minimal. One can conclude that the properties of the compound studied are determined mainly by the $d_{x^2-y^2}$ and d_{z^2} orbitals.

3.2.6. Fermi surfaces

The Fermi surfaces calculated in the first Brillouin zone are displayed in Fig. 10. The surfaces are plotted along the indicated high symmetry points. The hole-like Fermi surface sheets in the form of concentric cylinders are seen [Fig. 10(a)] in the central region of the Brillouin zone and along the Γ−Z direction. The hole pockets at the center of the Brillouin zone are not of the same size. Upon careful inspection of Fig. 10(a) one realizes that there is a small dispersion along k_z which increases at the outermost Fermi surface. The Fermi surface sheets are wider in diameter at Γ and become smaller towards Z in both directions. The four corners of the Brillouin zone consist of the Fermi surface sheets of the electron-like character, i.e., the electron pockets are aligned parallel to the A−M direction.

Similar features can be seen in the Fermi surfaces for the spin-down configuration [Fig. 10(b)]. The only difference is in the density of the Fermi surface sheets. This difference results from the fact that the bands for the spin-up configuration are more closely packed along the Fermi level than those for the spin-down configuration. The same Fermi surface topologies have been found in similar Fe-based superconductors [14–16].

3.2.7. Magnetic moments and Mössbauer hyperfine parameters

The calculated magnetic moment per formula unit of $CsEuFe_4As_4$ is 6.816 μ_B. This value consists of the contribution from the muffin-tin and the interstitial (0.2058 μ_B) regions. The calculated magnetic moments carried by the Cs, Eu, Fe, As_1, and As_2 atoms are 0.00, 6.91, − 0.07, 0.00, and − 0.01 μ_B, respectively. The calculated Eu magnetic moment is somewhat greater than the experimental moment of 5.9 μ_B at 2 K [4] that was derived from the magnetization measurements. The nearly vanishing calculated magnetic moment of the Fe atoms is in excellent agreement with the experimental observation via ^{57}Fe Mössbauer spectroscopy [6] of a zero intrinsic magnetic moment of the Fe atoms down to 2.1 K. The values of the calculated magnetic moments indicate that ferromagnetism in $CsEuFe_4As_4$ is associated exclusively with the Eu atoms.

Three types of the hyperfine-interaction parameters can be derived from the fits of Mössbauer spectra [17]. These are: the isomer shift δ_0, the principal component of the electric field gradient tensor V_{zz} and the asymmetry parameter η, and the hyperfine magnetic field H_{hf}. They can

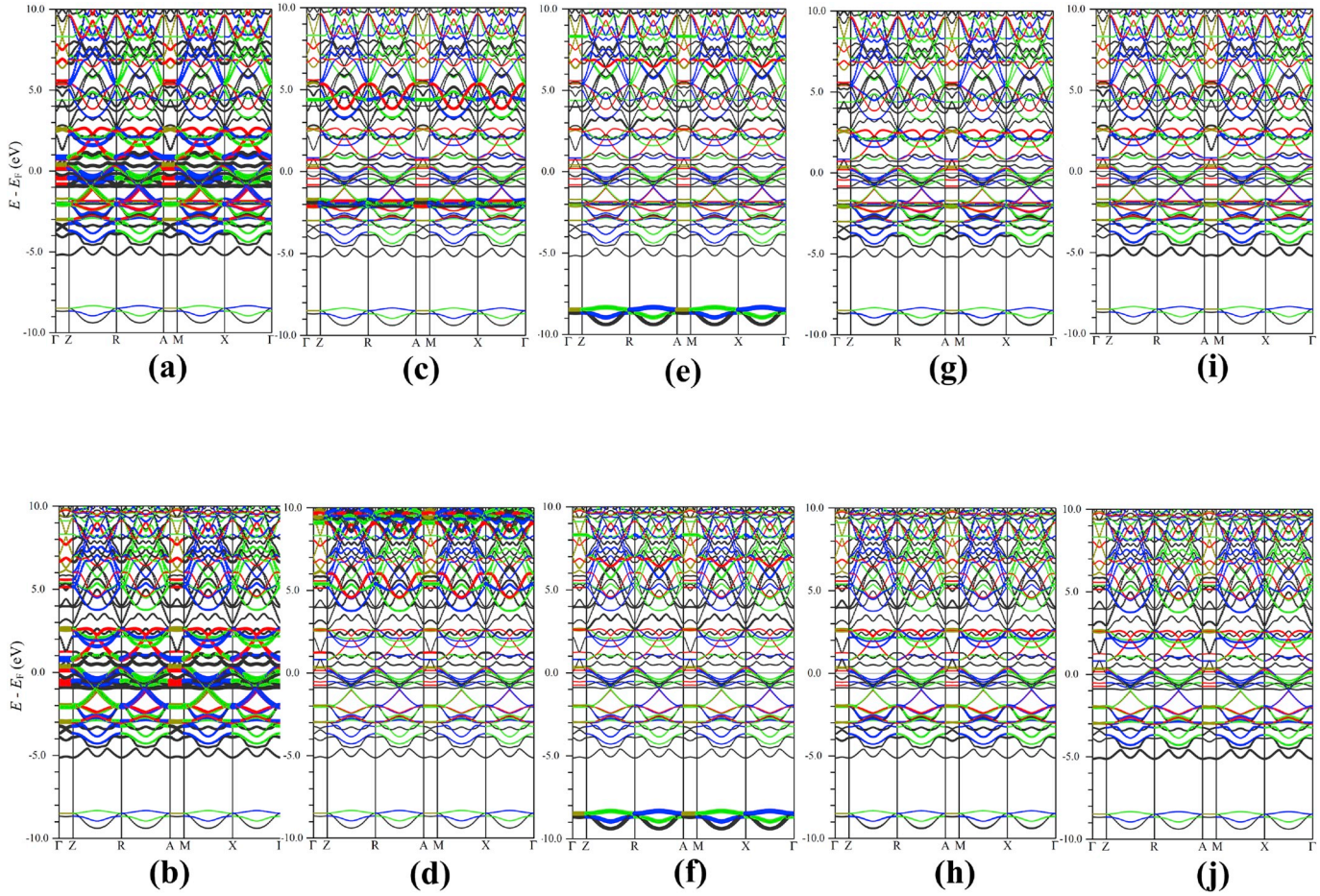

Fig. 8. (Color online) Spin-polarized and atom-resolved band structure of ferromagnetic $CsEuFe_4As_4$. The Fe spin-up (a) and spin-down (b) contributions. The Eu spin-up (c) and spin-down (d) contributions. The Cs spin-up (e) and spin-down (f) contributions. The As_1 spin-up (g) and spin-down (h) contributions. The As_2 spin-up (i) and spin-down (j) contributions. (For interpretation of the references to colour in this figure legend, the reader is referred to the Web version of this article.)

also be obtained from *ab initio* calculations carried out for any crystalline compound with known crystal structure [18].

The isomer shift can be calculated from the expression $\delta_0 = \alpha[\rho(0) - \rho_{ref}(0)]$, where $\rho(0)$ and $\rho_{ref}(0)$ are, respectively, the total electron densities at the Mössbauer nucleus in the compound studied and in the reference material, and α is a calibration constant. In calculating $\rho(0)$, relativistic spin-orbit effects were included to account for the possibility of the penetration of the $p_{1/2}$ electrons into the ^{57}Fe nuclei [19]. The reference material for ^{57}Fe Mössbauer spectroscopy is α-Fe metal (with the *bcc* structure and the lattice constant of 2.8665 Å). The calculated $\rho(0)$ and $\rho_{ref}(0)$ are 15308.539 and 15309.918 (a. u.)$^{-3}$, respectively. Using the calibration constant $\alpha = -0.291$(a. u.)^3(mm/s) [20], the calculated values of $\rho(0)$ and $\rho_{ref}(0)$ imply that $\delta_0 = 0.401$ mm/s (analogous calculations of δ_0 for ^{151}Eu Mössbauer spectra cannot be done as the corresponding α has not been established yet). The calculated δ_0 is close to the experimental value of 0.491 (1) mm/s [6].

The measured H_{hf} consists of three main contributions [21]: the Fermi contact term H_c, the magnetic dipolar term, H_{dip}, and the orbital moment term, H_{orb} [17]. The first term is generally much greater in magnitude than the other two terms. The Fermi contact term is calculated from the expression $H_c = \frac{8\pi}{3}\mu_B^2(\rho_\uparrow(0) - \rho_\downarrow(0))$, where $\rho_\uparrow(0)$ and $\rho_\downarrow(0)$ are the spin-up and spin-down densities at the Mössbauer nucleus, respectively. The calculated magnitudes of H_c at the ^{57}Fe and ^{151}Eu nuclei are 8.1 and 264.6 kOe, respectively. These should be compared with the corresponding experimental H_{hf} values (at 0 K) of 5.98 (13) and 272.9 (2.8) kOe [6].

The calculated V_{zz} and η are 7.142×10^{20} V/m^2 and 0.7795 for ^{57}Fe Mössbauer spectra [6]. The calculated V_{zz} and η imply that the value of the quadrupole splitting $\Delta = \frac{1}{2}eQ|V_{zz}|\sqrt{1+\eta^2/3}$ ($Q = 0.15$ b is the electric quadrupole moment of the 14.4-keV excited state of ^{57}Fe [22]) should be 0.1222 mm/s. For ^{151}Eu Mössbauer spectra, the calculated V_{zz} and η are -0.580×10^{22} V/m^2 and 0.0 (the zero value is consistent with the point symmetry 4/*mmm* of the Eu site). The experimental Δ (at 0 K) of 0.1182 mm/s [6] is in excellent agreement with the predicted value of 0.1222 mm/s. Similarly, good agreement is found between the calculated values of V_{zz} and η and the corresponding experimental values (at 0 K) of $-0.516(5) \times 10^{22}$ V/m^2 and 0.0 derived from the ^{151}Eu Mössbauer spectra [6].

4. Summary

We present the results of *ab-initio* calculations of the electronic structure, magnetism, and hyperfine interaction parameters of the new 35 K superconductor $CsEuFe_4As_4$. The calculations suggest the presence of a mixture of ionic, covalent, and metallic bonding between the constituent atoms. We discuss in detail the electronic band structure and the density of states. We show that, in agreement with the experimental results, the magnetic moment is due to the strongly localized Eu *f* states. We demonstrate that an almost zero magnetic moment carried by the Fe atoms results from an apparent symmetry of the spin-up and spin-down states. We find that Fermi surfaces have the hole-like and electron-like pockets located at the center and corners of the Brillouin zone, respectively. We show that the calculated ^{57}Fe and ^{151}Eu Mössbauer hyperfine interaction parameters are in good agreement with the corresponding parameters derived from the Mössbauer spectra.

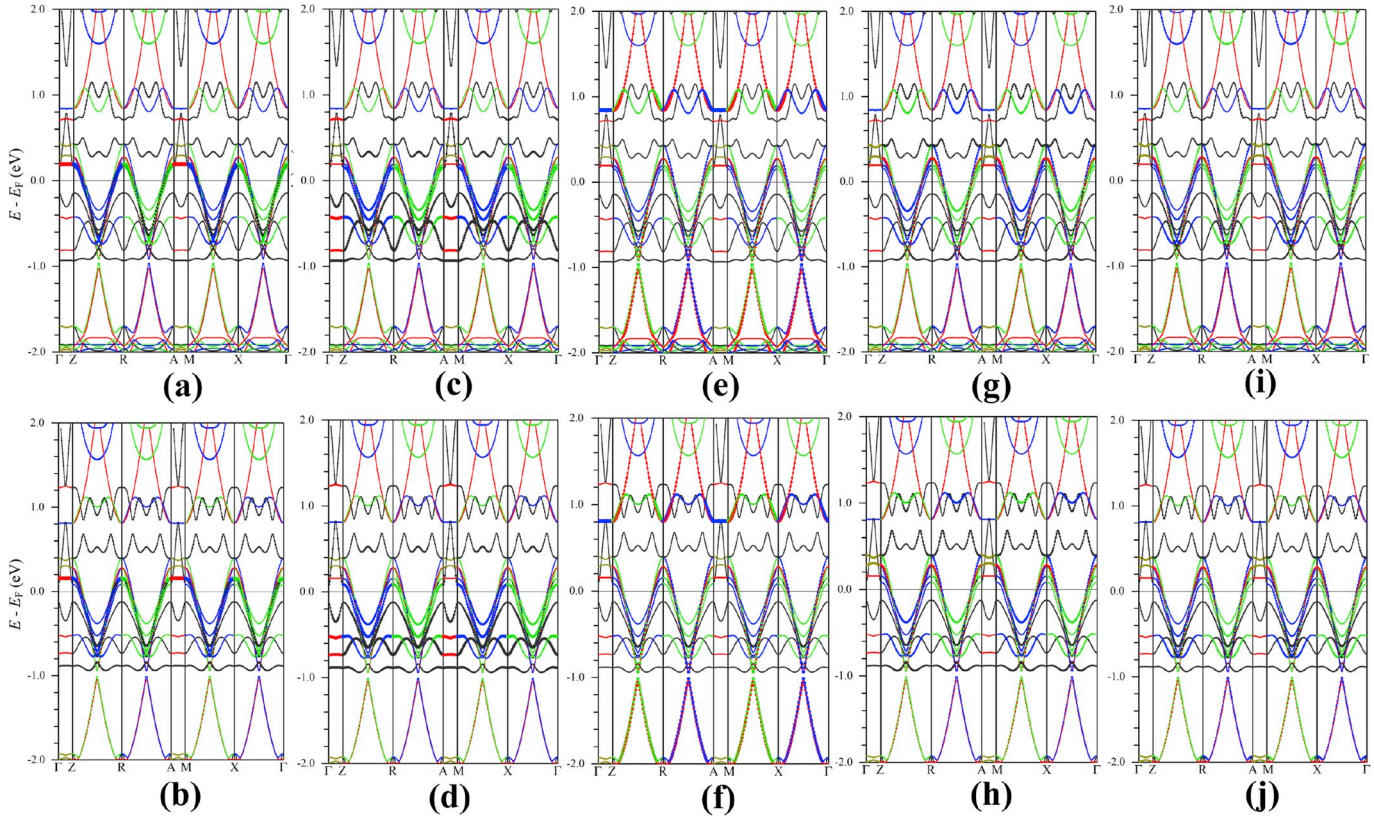

Fig. 9. (Color online) Spin-polarized band structure resulting from the Fe orbitals $d_{x^2-y^2}$ [(a), (b)], d_{z^2} [(c), (d)], d_{xy} [(e), (f)], d_{xz} [(g), (h)], and d_{yz} [(i), (j)]. (For interpretation of the references to colour in this figure legend, the reader is referred to the Web version of this article.)

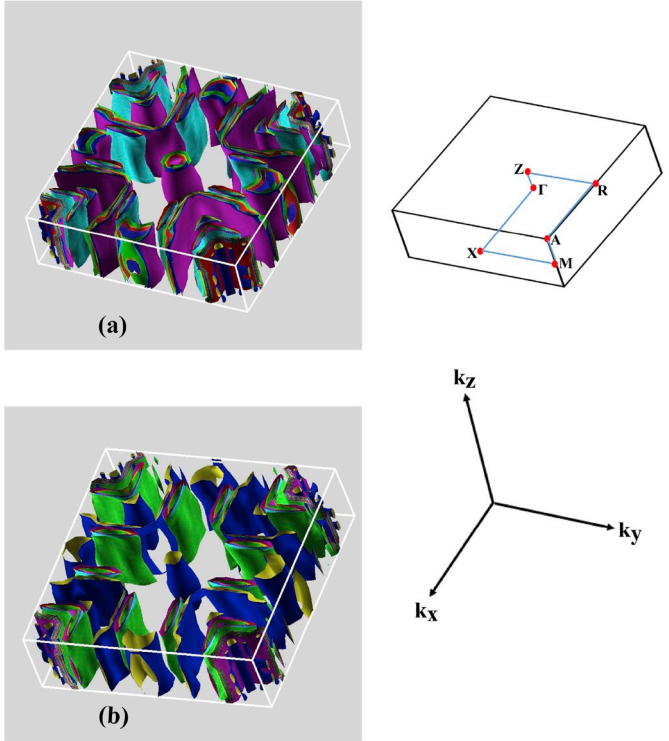

Fig. 10. (Color online) Fermi surfaces of the ferromagnetic $CsEuFe_4As_4$ for the spin-up (a) and spin-down (b) configurations. (For interpretation of the references to colour in this figure legend, the reader is referred to the Web version of this article.)

Acknowledgements

This work was supported by the Natural Sciences and Engineering Research Council of Canada (NSERC).

References

[1] A. Iyo, K. Kawashima, T. Kinjo, T. Nishio, S. Ishida, H. Fujihisa, Y. Gotoh, K. Kihou, H. Eisaki, Y. Yoshida, J. Am. Chem. Soc. 138 (2016) 3410.
[2] K. Kawashima, T. Kinjo, T. Nishio, S. Ishida, H. Fujihisa, Y. Gotoh, K. Kihou, H. Eisaki, Y. Yoshida, A. Iyo, J. Phys. Soc. Jpn. 85 (2016) 064710.
[3] Y. Liu, Y.-B. Liu, H. Jiang, Z.-C. Wang, A. Ablimit, W.-H. Jiao, Q. Tao, C.-M. Feng, Z.-A. Xu, G.-H. Cao, Phys. Rev. B 93 (2016) 214503.
[4] Y. Liu, Y.-B. Liu, Q. Chen, Z.-T. Tang, W.-H. Jiao, Q. Tao, Z.-A. Xu, G.-H. Cao, Sci. Bull. 61 (2016) 1213.
[5] L.N. Bulaevskii, A.I. Buzdin, M.L. Kulić, S.V. Panjukov, Adv. Phys. 34 (1985) 175 S. Zapf and M. Dressel, Rep. Prog. Phys. 80, 016501 (2017).
[6] M.A. Albedah, F. Nejadsattari, Z.M. Stadnik, Y. Liu, G.-H. Cao, J. Phys. Condens. Matter 30 (2018) 155803.
[7] C. Xu, Q. Chen, C. Cao, Commun. Phys. 2 (2019) 16.
[8] P. Blaha, K. Schwartz, G. Madsen, D. Kvasnicka, J. Luitz, WIEN2k, an Augmented Plane Wave Plus Local Orbitals Program For Calculating Crystal Properties, Technical Universität Wien, Austria, 1999 Karlheinz Schwarz.
[9] F. Nejadsattari, P. Wang, Z.M. Stadnik, Y. Nagata, T. Ohnishi, J. Alloy. Comp. 725 (2017) 1098.
[10] J.P. Perdew, S. Burke, M. Ernzerhof, Phys. Rev. Lett. 77 (1996) 3865.
[11] V.I. Anisimov, O. Gunnarsson, Phys. Rev. B 43 (1991) 7570 V. I. Anisimov, J. Zaanen, and O. K. Andersen, Phys. Rev. B 44, 943 (1991); V. N. Antonov, B. N. Harmon, and A. N. Yaresko, Phys. Rev. B 72, 085119 (2005).
[12] R.F.W. Bader, Atoms in Molecules: A Quantum Theory, Oxford University Press, Oxford, 1991.
[13] P.E. Blöchl, O. Jepsen, O.K. Andersen, Phys. Rev. B 49 (1994) 16223.
[14] X. Shi, G. Wang, J. Phys. Soc. Jpn. 85 (2016) 124714.
[15] F. Lochner, F. Ahn, T. Hickel, I. Eremin, Phys. Rev. B 96 (2017) 094521.
[16] D.V. Suetin, I.R. Shein, J. Supercond. Nov. Magnetism 31 (2018) 1683.
[17] N.N. Greenwood, T.C. Gibb, Mössbauer Spectroscopy, Chapman and Hall, London,

1971 P. Gütlich, E. Bill, and A. Trautwein, Mössbauer Spectroscopy and Transition Metal Chemistry (Springer, Berlin, 2011).
[18] P. Blaha, J. Phys. Conf. Ser. 217 (2010) 012009.
[19] F. Nejadsattari, Z.M. Stadnik, J. Żukrowski, J. Alloy. Comp. 639 (2015) 547.
[20] U.D. Wdowik, K. Reubenbauer, Phys. Rev. B 76 (2007) 155118.
[21] F. Nejadsattari, Z.M. Stadnik, J. Przewoźnik, K.H.J. Buschow, Physica B 477 (2015) 113.
[22] G. Martínez-Pinedo, P. Schwerdtfeger, E. Caurier, K. Langanke, W. Nazarewich, T. Söhnel, Phys. Rev. Lett. 87 (2001) 062701.